Redistribution of Velocity and Bed-Shear Stress in Straight and Curved Open Channels by Means of a Bubble Screen: Laboratory Experiments

K. Blanckaert[1]; F. A. Buschman[2]; R. Schielen[3]; and J. H. A. Wijbenga[4]

Abstract: Open-channel beds show variations in the transverse direction due to the interaction between downstream flow, cross-stream flow, and bed topography, which may reduce the navigable width or endanger the foundations of structures. The reported preliminary laboratory study shows that a bubble screen can generate cross-stream circulation that redistributes velocities and hence, would modify the topography. In straight flow, the bubble-generated cross-stream circulation cell covers a spanwise extent of about four times the water depth and has maximum transverse velocities of about 0.2 ms^{-1}. In sharply curved flow, it is slightly weaker and narrower with a spanwise extent of about three times the flow depth. It shifts the counter-rotating curvature-induced cross-stream circulation cell in the inwards direction. Maximum bubble-generated cross-stream circulation velocities are of a similar order of magnitude to typical curvature-induced cross-stream circulation velocities in natural open-channel bends. The bubble screen technique is adjustable, reversible, and ecologically favorable. Detailed data on the 3D flow field in open-channel bends is provided, which can be useful for validation of numerical models.

DOI: 10.1061/(ASCE)0733-9429(2008)134:2(184)

CE Database subject headings: Open channels; Bending; Secondary flow; Bubbles; Experimentation; Shear stress; Velocity; Curvature.

Introduction

The bed in open channels is seldom flat, but shows important variations in the transverse direction. Alternating bars often develop in straight flow (Jaeggi 1984) and a more pronounced bar-pool topography in curved flow among others (Fargue 1868; Chow 1959; Odgaard 1981; Whiting and Dietrich 1993). These variations in bed topography are of practical relevance. The navigable width is reduced over shoals, and foundations of structures such as bridge piers, abutments, or bank protection may be endangered in the deeper parts.

These macrobed topography features are due to an intricate interaction between the downstream flow, the cross-stream flow, that is defined as flow perpendicular to the channel axis, and the bed topography among others (Schielen et al. 1993; Knaapen et al. 2001) for straight flow and among others (Engelund 1974; Kikkawa et al. 1976; Odgaard 1984; Ikeda and Nishimura 1985; Struiksma 1985) for curved flow. The bed topography is mainly shaped by the distribution of the bed-shear stress, which is determined by the velocity distribution [cf. Eq. (1) in Section "Experimental Results"]. This velocity distribution may be attributed to two phenomena: (1) advective transport of downstream momentum by the cross-stream flow; (2) the bed topography itself, since a deeper flow depth attracts higher velocities according to Chézy's law.

This interaction is especially important in open-channel bends, which are characterized by an important curvature induced cross-stream circulation [among others (Thomson 1876; Rozovskii 1957; de Vriend 1977)], also called secondary flow, helical flow, or spiral flow, and a bar-pool bed topography with pronounced transverse slopes of the bed among others (Fargue 1868; Odgaard 1981; Whiting and Dietrich 1993). Different techniques have been investigated and applied to modify the bed topography in open-channel bends, mainly in order to reduce bend scour or to enlarge the navigable width. They can be divided into techniques that directly act upon the bed topography, indirect techniques that modify the flow field, and combinations of both:

- An example of a technique that directly acts upon the bed topography is the filling of the pool of a bend and its covering with a nonerodible fixed layer. This induces a flow redistribution that causes an increase of flow velocity over the point bar, forcing erosion at the inner bend. Moreover, the fixed layer reduces transverse sediment transport from the pool zone in the outer bend towards the point bar in the inner bend (Sloff et al. 2006). This technique has been applied in the Netherlands in bends on the River Waal near St-Andries and the bend upstream of Nijmegen (cf. Fig. 11 in section "Discussion") in order to enlarge the navigable width. Due to long-term morphological lowering of the river bed, however, a construction such as a fixed layer may become an obstacle for shipping.
- The use of a horizontal foundation of the outer bank that pro-

[1]ICARE-ENAC, Ecole Polytechnique Fédérale, CH-1015 Lausanne, Switzerland; and, Faculty of Civil Engineering and Geosciences, Delft Univ. of Technology, The Netherlands. E-mail: koen.blanckaert@epfl.ch

[2]Hydrology and Quantitative Water Management Group, Wageningen Univ., Nieuwe Kanaal 11, 6709 PA Wageningen, The Netherlands.

[3]Ministry of Transport, Public Works and Water Management, Institute for Inland Water Management and Waste Water Treatment, P.O. Box 9072, 6800 ED Arnhem, The Netherlands.

[4]HKV Consultants, P.O. Box 2120, 8203AC Lelystad, The Netherlands.

Note. Discussion open until July 1, 2008. Separate discussions must be submitted for individual papers. To extend the closing date by one month, a written request must be filed with the ASCE Managing Editor. The manuscript for this paper was submitted for review and possible publication on August 8, 2006; approved on June 1, 2007. This paper is part of the ***Journal of Hydraulic Engineering***, Vol. 134, No. 2, February 1, 2008. ©ASCE, ISSN 0733-9429/2008/2-184–195/$25.00.

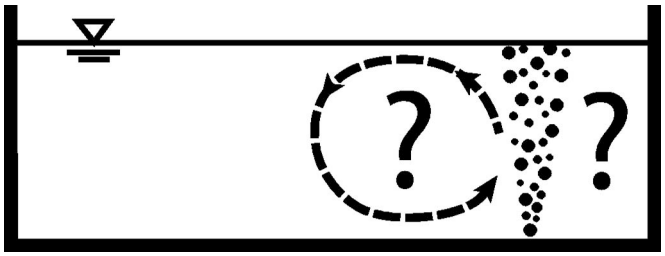

Fig. 1. Conceptual sketch of the bubble technique

trudes into the flow reduces the scour depth in bends by modifying the flow field and directly acting upon the bed (Roca et al. 2006).

- The application of macroroughness elements at the outer bank aims to shift the core of the high downstream velocities away from the bank, hence reducing bend scour (Hersberger 2002).
- Bottom vanes installed on the bed intend to generate a cross-stream circulation that counteracts the curvature induced one and hence reduce the pronounced curvature induced bend topography (Odgaard and Spoljaric 1986; Odgard and Wang 1991). Such vanes have successfully been applied, but their major drawback is that they are dangerous obstacles for shipping.

Fig. 1 shows a conceptual sketch of the technique investigated in this paper: Rising air bubbles entrain a vertical motion of the fluid, which could trigger the formation of a cell of cross-stream circulation away from the bubble screen. It is not a priori clear how the flow field between the bubble screen and the bank would be affected. This technique has the major advantage of being reversible, adjustable, and ecologically favorable.

This paper reports a preliminary investigation on the use of bubble screens in open channels that addresses the following questions:

- Can a bubble screen trigger the development of a cross-stream circulation cell?
- What are the characteristics, such as the intensity or the spanwise extent, of such a bubble generated cross-stream circulation cell?
- How do the bubble and curvature-generated cross-stream circulation cells interact?
- Is the bubble screen technique technically and economically feasible?

In addition, this paper provides detailed experimental data on the three-dimensional velocity field in straight and sharply curved flows that may be useful for the validation of numerical codes.

This paper will first present the experimental setup and the framework of the analysis. Subsequently, experiments in a straight flow are presented that address the first and second of the above questions. Finally, curved flow experiments are presented and the results are discussed.

Experiments

Experiments have been carried out in the laboratory flume at Ecole Polytechnique Fédérale Lausanne (EPFL) shown in Fig. 2 and described in detail by Blanckaert (2002). It consists of a 9 m long straight inflow reach, followed by a 193° bend of constant centerline radius of curvature of $R=1.7$ m and a 5 m long straight outflow reach. The width was constant at $B=1.3$ m, and cross

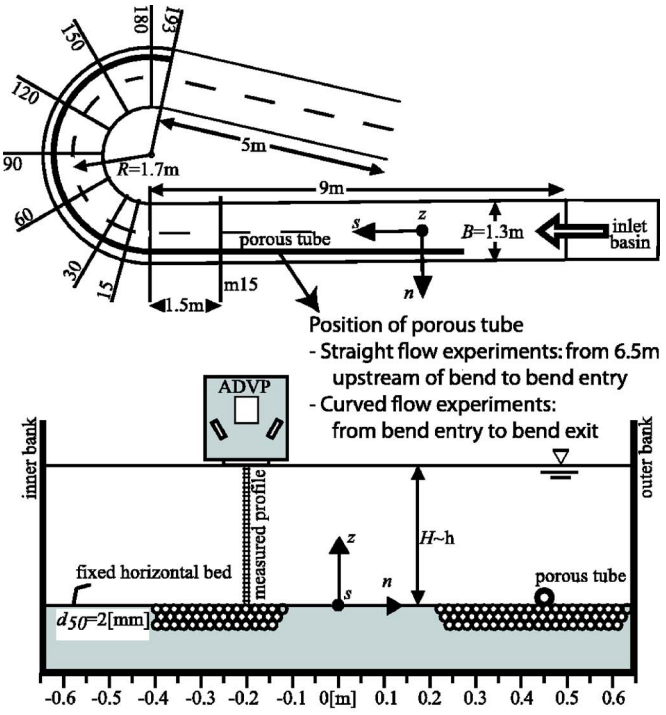

Q [l/s]	H [m]	U [m/s]	$(g/C_f)^{1/2}$ [$m^{1/2}$ s^{-1}]	Re [10^3]	Fr [/]	R/B [/]	H/R [/]	B/H [/]
89	0.159	0.43	34	69	0.35	1.31	0.094	8.2

Fig. 2. Experimental setup, reference system, ADVP, and hydraulic conditions. Q=discharge; H=flume-averaged flow depth; $U=Q/(BH)$=flume-averaged velocity; $(g/C_f)^{1/2}$=Chézy type friction factor; $\mathrm{Re}=UH/v$=Reynolds number; $\mathrm{Fr}=U/\sqrt{gH}$=Froude number.

sections were rectangular. This simple geometry allows the focus to be on the effects of the bubble screen on the flow, without contamination by the effects of a complex mobile bed morphology. The bed and the outer bank were composed of glued quasi-uniform sediments with a mean diameter of $d=0.002$ m, and the inner bank was made of Plexiglass. A downstream bed slope of 0.22% was installed in the straight inflow reach, and the bed was horizontal in the rest of the flume.

An orthogonal curvilinear (s,n,z) reference system was adopted, where the downstream s axis coincides with the flume's centerline, the transverse n axis points in the outward direction, and the vertical z axis is upwards.

The hydraulic conditions are listed in Fig. 2. The flume-averaged water depth of $H=0.159$ m was chosen in order to optimize the application of the measuring instruments. This led to a subcritical flow with $\mathrm{Fr}=0.35$. The experimental setup and hydraulic conditions are similar to previous experiments by Blanckaert (2002), which facilitates interpretation of the results. The implications of the depth to radius ratio of $H/R=0.094$ and width to depth ratio of $B/H=8.2$, indicative of a rather narrow sharply curved bend, will be discussed in the section "Discussion."

The bubble screen is generated by means of a porous tube, installed on the bed from 6.5 m upstream of the bend to the bend entry to investigate its effect in straight flow, and from the bend entry to the bend exit to investigate its effect in curved flow (Fig. 2). It was positioned at 0.2 m from the outer bank of the flume (Fig. 2), since at this location, maximum downward

velocities ($v_z<0$) were measured in the bend reach in the reference experiments without the bubble screen (cf. Fig. 6). Pressurized air is introduced at both ends of the porous tube, resulting in a quasi-uniform bubble generation along the tube. During their rise in the water column, the bubbles spread laterally and occupy a flow region of about 0.2 m wide ($n=0.35$ to 0.55 m at the water surface, where the generated bubbles had a diameter in the range of 0.002 to 0.015 m, with an average of about 0.005 m.

The rising air bubbles entrain a vertical ascending motion of the fluid $v_z>0$, which is mainly determined by the vertical momentum of the bubble screen, hence, the flux of air times its rising velocity:

- In the first approximation, the flux of air introduced in the flow is proportional to the applied pressure, which can be adjusted.
- The rising velocity is determined by buoyancy effects, since kinetic energy effects are probably negligible given the ratio of water to air density. The equilibrium rising velocity of bubbles in the relevant size range is about constant at 0.24 ms^{-1} and does not depend on the flow depth or velocity (Leifer et al. 2000).

The generation of a cross-stream circulation cell by the bubble screen seems to be triggered by the principle of mass conservation. The rising air bubbles entrain upward velocities $v_z>0$. However, at the bed and the water surface, the kinematic boundary condition imposes zero vertical fluid velocity. According to the mass conservation equation, the gradient in vertical velocity $\partial v_z/\partial z$ generates transverse velocities, which are a maximum near the bed and the water surface, and hence generates a cross-stream circulation cell. It is not clear, however, what mechanisms control the spanwise extent of this bubble-induced cell.

Vertical profiles of the 3D velocity vector (v_s, v_n, v_z) were measured with an acoustic Doppler velocity profiler (ADVP) placed in a housing that touches the water surface as illustrated in Fig. 2. The induced flow perturbation in a layer of about 0.02 m required that this near-surface region be bridged by means of extrapolations [reported in Blanckaert and Graf (2001)] for the calculation of depth-averaged flow quantities. This leads to an additional uncertainty of about 5% in these depth-averaged flow quantities, which, however, does not alter the interpretation and conclusions of the results.

The working principle of the ADVP, data treatment procedures and estimations of the accuracy in the flow variables have been reported by Lemmin and Rolland (1997), Hurther and Lemmin (1998), Blanckaert and Graf (2001), Blanckaert and de Vriend (2004), and Blanckaert and Lemmin (2006). Acquisition time was 180 s and measurements were made in the cross sections 1.5 m upstream of the bend and at 15, 30, 60, 90, 120, 150, and 180° in the bend. Vertical profiles were measured in each cross section every 0.1 m in the range $n=-0.5$ m to $n=0.5$ m, except for the cross sections 1.5 m upstream of the bend and the cross section with maximum cross-stream circulation (see further) at 90° in the bend, which were measured on the refined grid including verticals at $n=[-0.5, -0.475, -0.45, -0.425, -0.4, -0.375, -0.35, -0.325, -0.3, -0.25, -0.2, -0.15, -0.1, -0.05, 0, 0.05, 0.1, 0.15, 0.2, 0.25, 0.3, 0.325, 0.35, 0.375, 0.4, 0.425, 0.45, 0.475, 0.5]$ m. In the presence of the bubble screen, the high air concentration did not allow reliable measurements in the region $n>0.3$ to 0.4 m. This flow region is being investigated by means of numerical simulations.

Experimental Results

Flow Parameters

The bed topography is mainly shaped by the distribution of the bed-shear stress τ_b, which is determined by the velocity distribution. In a first approximation, the bed-shear stress can be estimated from the distribution of the depth-averaged downstream velocity $U_s=\langle v_s \rangle$ by means of a Chézy type relation

$$\tau_b = \rho C_f U_s^2 \tag{1}$$

As aforementioned, advective momentum transport by the cross-stream flow (v_n, v_z) is the predominant mechanism with respect to the redistribution of the velocities and the bed-shear stress. The cross-stream flow can be decomposed into cross flow $U_n=\langle v_n \rangle$ representing translatory motion, and cross-stream circulation (v_n^*, v_z) representing circulatory motion (Bradshaw 1987)

$$\begin{cases} v_s = U_s + v_s^* \\ v_n = U_n + v_n^* \\ v_z \end{cases} \tag{2}$$

Note that brackets $\langle\ \rangle$ indicate depth-averaged values and an asterisk indicates the local deviations from the depth-averaged values. The cross-stream circulation pattern is well visualized by means of the function ψ, defined as

$$\psi = \frac{1}{2}(\psi_n + \psi_z)$$

$$\psi_n = -(1 + n/R)\int_{z_b}^{z} v_n^* dz$$

$$\psi_z = \int_{-B/2}^{n} (1 + n/R) v_z dn + cte \tag{3}$$

z_b represents the bed elevation and the integration constant in Eq. (3) is chosen such that the cross-sectional averaged values of ψ_n and ψ_z are equal. In fully-developed curved flow ($\partial/\partial s=0$, infinite bend), $\psi_n=\psi_z$ and ψ represents the classical definition of the streamfunction (Batchelor 1967), therefore the function ψ will be called the pseudostreamfunction hereafter. This pseudostreamfunction has the advantage of being a scalar quantity, in contrast to the cross-stream circulation vector (v_n^*, v_z).

Straight Flow

Measurements were carried out in the cross section 1.5 m upstream of the bend where the boundary layer is fully developed and no bend effects are felt. The porous tube was installed from 6.5 m upstream of the bend to the bend entrance at 0.2 m from the outer bank. These experiments aimed to:

- Analyze if a bubble screen can trigger a well-defined cross-stream circulation cell,
- Analyze the relationship between the bubble-generated flow pattern and the introduced air flux,
- Provide reference data on the pattern of cross-stream circulation (extent, intensity, etc.) for comparison to the curved-flow experiments.

Experiments were conducted with the pressure applied to the porous tube ranging from 100 to 600 kPa in increments of 50 kPa, resulting in the volume air fluxes per unit m of porous tube length of [0.059, 0.087, 0.113, 0.138, 0.161, 0.184, 0.205,

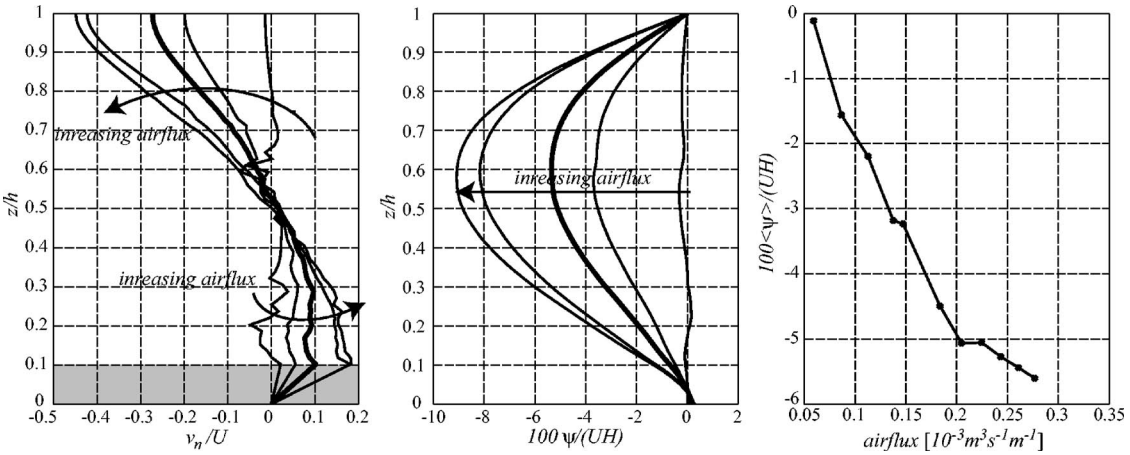

Fig. 3. Measurements in the centerline in the straight reach. Results as function of introduced air flux; results shown for air fluxes of [0.059, 0.113, 0.161, 0.205, 0.277] 10^{-3} m^3 s^{-1} m^{-1}: (a) profiles of the normalized transverse velocity component v_n/U; (b) profiles of the normalized pseudostreamfunction $100\psi/(UH)$; and (c) normalized depth-averaged pseudostreamfunction $100\langle\psi\rangle/(UH)$. Profiles for an airflux of 0.161 m^3 s^{-1} m^{-1} in (a) and (b) are indicated with a bold line.

0.225, 0.243, 0.261, 0.277] 10^{-3} m^3 s^{-1} m^{-1}, respectively. For these air fluxes, velocity profiles were measured at the centerline of the flume. The evolution of the cross-stream flow pattern as a function of the air flux is illustrated by means of the normalized transverse velocity component v_n/U [Fig. 3(a)], the corresponding normalized pseudostreamfunction $100\psi/(UH)$ [Fig. 3(b)] and the depth-averaged normalized pseudostreamfunction $100\langle\psi\rangle/(UH)$ [Fig. 3(c)].

The measured profiles show convincingly that the bubble screen triggers the generation of a cross-stream circulation cell, which strengthens with increasing air flux. The velocities away from the bubble screen near the water surface are significantly higher than the velocities towards the bubble screen near the bed. The corresponding mass flux away from the bubble screen is indicative of advective velocity redistribution away from the bubble screen.

The amplitude of the cross-stream circulation increases approximately linearly at low air fluxes. The increase slows down, however, with increasing air supply. More details of the cross-stream circulation were observed for an air flux of 0.161 10^{-3} m^3 s^{-1} m^{-1}, which is situated in the linear range and generated by an air pressure of 300 kPa that corresponds to the working pressure of the porous tube as provided by the manufacturer.

The velocity pattern was measured in the entire cross section in the presence of this bubble screen. The generated patterns of cross-stream flow and cross-stream circulation are illustrated by means of the $(v_n, v_z)/U$ vector [Fig. 4(a)] and the normalized pseudostreamfunction, $100\psi/(UH)$ [Fig. 4(b)], respectively.

The bubble generated cross-stream circulation cell covers the region $n=-0.2$ m to 0.45 m, hence its width corresponds to about four times the flow depth. Its core is found at about $n=0.25$ m with a maximum value of $100\psi/(UH)=-11.5$, a maximum depth-averaged value of $100\langle\psi\rangle/(UH)=-6$ and corresponding maximum inward and outward transverse velocities of about -0.2 and 0.1 ms^{-1}, respectively.

Advective momentum transport by this cross-stream circulation modifies the downstream velocity distribution (de Vriend 1981; Blanckaert and Graf 2004). Without the bubble screen, the normalized downstream velocity v_s/U is quite uniformly distributed over the width [Fig. 5(a)]. The relatively weak span-

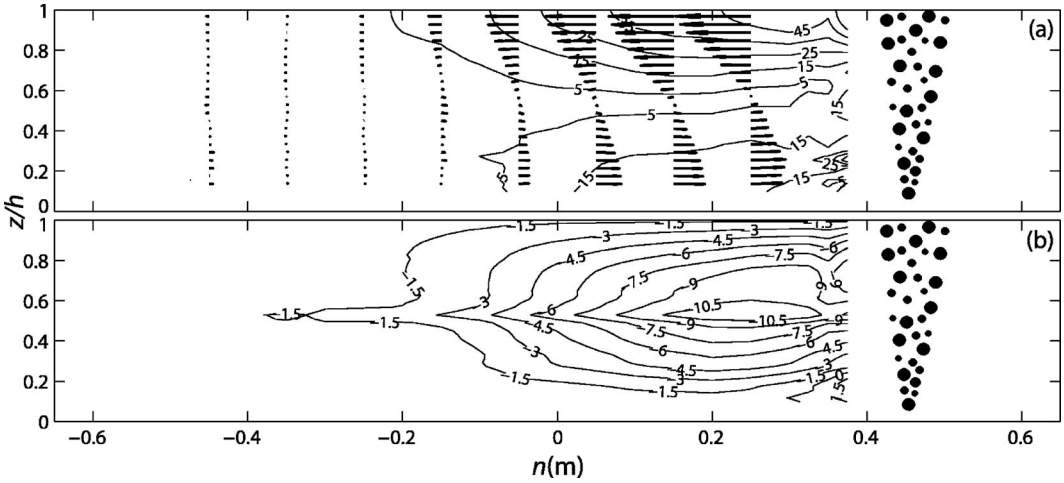

Fig. 4. Bubble-screen induced cross-stream flow and cross-stream circulation in the straight reach: (a) normalized vector representation $(v_n, v_z)/U$. The isolines show the magnitude of the vector in [%]; (b) normalized pseudostreamfunction, $100\psi/(UH)$.

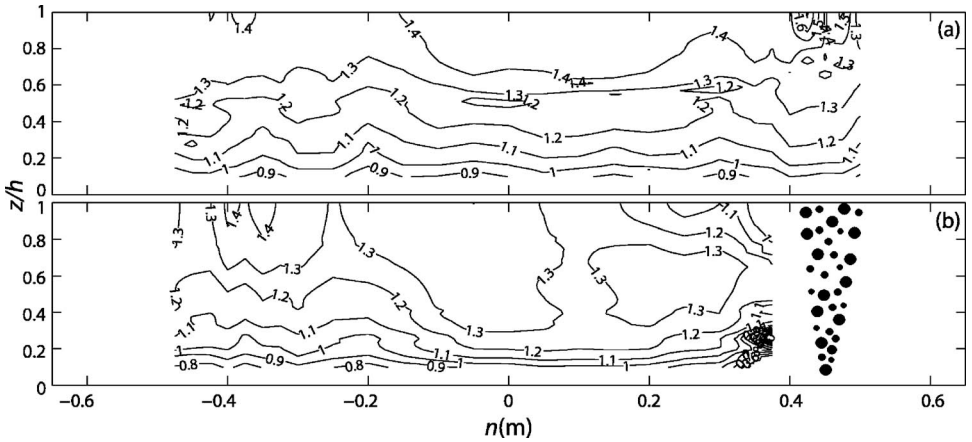

Fig. 5. Distribution of the normalized downstream velocity v_s/U in the straight reach: (a) without the bubble screen; (b) with the bubble screen

wise variations, suggesting alternating regions of upflow ($v_z>0$) and downflow ($v_z<0$) can be attributed to weak cross-stream circulation cells induced by turbulence anisotropy (Nezu and Nakagawa 1984, 1993; Colombini 1993).

In the presence of the bubble screen, the downstream velocity distribution is significantly modified in the flow region covered by the cross-stream circulation cell [Fig. 5(b)]. In the upflow region ($n=0.3$ to 0.45), low near bed velocities are conveyed in upward direction and subsequently spread out by the inward transverse velocities near the water surface. In the downflow region ($n=-0.2$ to 0.2), high near surface velocities are conveyed towards the bed and subsequently spread out in outward direction by the transverse velocities.

Curved Flow

Measurements were carried out in the cross sections at 15, 30, 60, 90, 120, 150, and 180° round the bend in a reference experiment and in an experiment with a bubble screen, generated by means of the porous tube installed from the bend entry to the bend exist and providing a volume air flux of 0.161 10^{-3} m^3 s^{-1} m^{-1}. These experiments aimed to:

- Analyze and compare the patterns of cross-stream circulation in the reference experiment and the experiment with the bubble screen.
- Compare the patterns of the bubble induced cross-stream circulation cell in straight and curved flow.
- Analyze the interaction between the curvature and bubble induced cross-stream circulation cells.
- Analyze and compare the patterns of the downstream velocity and the bed-shear stress in the reference experiment and the experiment with the bubble screen.

The characteristics of the cross-stream circulation in the experiments with and without the bubble screen are illustrated in Fig. 6 by means of the patterns of normalized pseudostreamfunction, $100\psi/(UH)$ in the measured cross sections and in Fig. 7 by means of the distribution of the normalized depth-averaged pseudostreamfunction $100\langle\psi\rangle/(UH)$ in the bend reach.

In the reference experiment without the bubble screen, the cross-stream circulation pattern typical for open-channel bends develops. A curvature-induced cell of cross-stream circulation, called the center-region cell, develops upon entering the bend reach. It reaches its maximum strength of $100\psi/(UH)\approx 10$ and $100\langle\psi\rangle/(UH)\approx 7$ in the cross section at 90° and subsequently significantly decays in the second half of the bend (Fig. 7). The core of the cross-stream circulation cell, indicated by the maximum values, is found in the outer half of the cross sections. An outer-bank cell of reverse cross-stream circulation is discernible near the outer-bank downstream from the cross section at 60°, where it covers the flow region $n=0.4$ to 0.65 m in the upper part of the water column (Fig. 6). Its maximum strength is about $100\psi/(UH)=-4$ at the edge of the measuring grid. Such outer-bank cells have been measured and analyzed in detail by Blanckaert and Graf (2001), Blanckaert (2002), and Blanckaert and de Vriend (2004). In a similar experiment with smooth Plexiglass outer bank, Blanckaert (2002) measured a center-region cell of comparable strength, but a significantly weaker outer-bank cell.

In the presence of the bubble screen, a bubble generated cross-stream circulation cell develops. The curvature induced circulation cell is crushed in the inwards direction (Fig. 6). The bubble generated cross-stream circulation cell strengthens and widens in downstream direction upon entering the bend. It reaches its maximum strength of $100\psi/(UH)\approx -11$ and $100\langle\psi\rangle/(UH)\approx -6.0$ in the cross section at 90°, with corresponding maximum inward and outward transverse velocities of about −0.2 and 0.1 ms^{-1}, respectively. Subsequently it decays, which may be attributed to the widening of the cell. The maximum spanwise extent of $n=0$ to 0.45 m is reached in the cross section at 120°, where the strength is reduced to $100\langle\psi\rangle/(UH)\approx -2$. Downstream from this cross section, the bubble generated cross-stream circulation cell remains approximately stable.

The bubble generated cross-stream circulation cell is only slightly weaker in curved flow than in straight flow. Its transverse development, however, is hindered by the presence of the curvature induced cross-stream circulation cell, and its spanwise extent is reduced to about three times the flow depth.

This bubble generated cross-stream circulation cell crushes the curvature induced cell in the inwards direction, but only slightly reduces its maximum strength of $100\psi/(UH)\approx 9$ and $100\langle\psi\rangle/(UH)\approx 6$, which still occurs in the cross section at 90° (Figs. 6 and 7). The decay of the curvature induced cell in the second part of the bend, however, is accentuated (Fig. 7). This may tentatively be attributed to the interaction between the downstream velocity distribution and the cross-stream circulation (Blanckaert and de Vriend 2003).

The interaction between both circulation cells, thus, hardly modifies their strength and development, but mainly reduces their spatial extent. Vertical downstream velocities are amplified at the

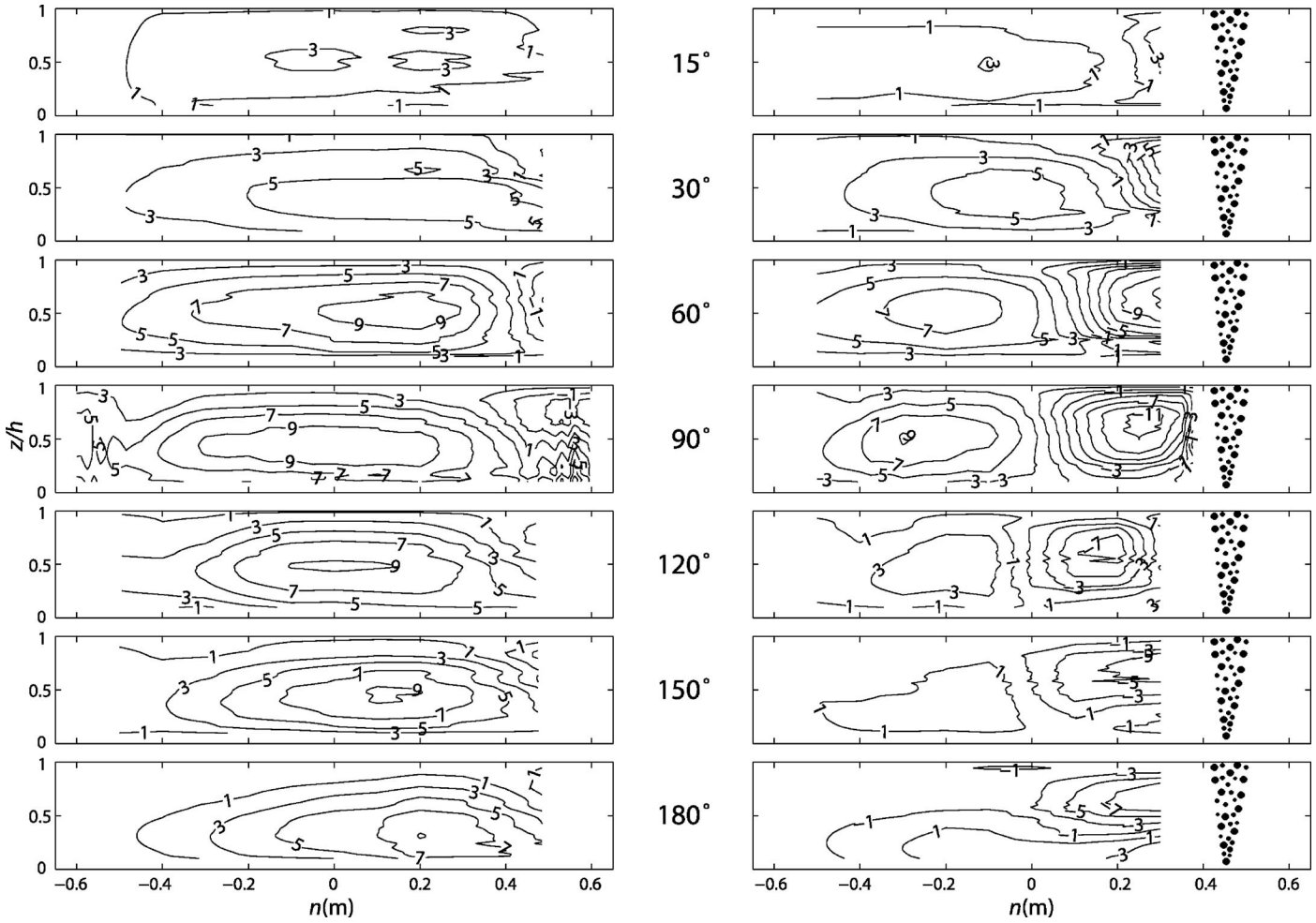

Fig. 6. Patterns of normalized pseudostreamfunction, $100\psi/(UH)$, measured in the cross sections at 15, 30, 60, 90, 120, 150, and 180° without (left column) and with the bubble screen (right column)

junction between both cells. Remarkably, both circulation cells have a similar downstream evolution and reach their maximum intensity in the same cross section.

Advective momentum transport by these cross-stream circulation cells determines the distribution of the downstream velocities and the bed-shear stress (de Vriend 1981; Blanckaert and Graf 2004), as illustrated in Figs. 8 and 9 for the experiments with and without the bubble screen.

Fig. 8 shows the distribution of the downstream bed-shear stress component τ_{bs} estimated according to Eq. (1), and normalized by means of the flume averaged bed-shear stress $\langle\langle\tau_b\rangle\rangle=\rho C_f U^2$ where $U=Q/(BH)$ is the flume averaged velocity.

Due to the potential vortex effect, the core of maximum bed-shear stress is found at the inner bank near the bend entry in both experiments. In the reference experiment without the bubble screen, the core of maximum bed-shear stress gradually shifts in the outwards direction around the bend, to be found at $n=0.3$ in the outer half of the cross section at 180° near the bend exit (Fig. 8). In the presence of the bubble screen, this outward shift is attenuated. The core of maximum bed-shear stress does not migrate further outward than the junction of both circulation cells, which is found near the centerline, and the bed shear stress decreases towards both banks (Fig. 8). The maximum value of the bed-shear stress is higher in the presence of the bubble screen. This maximum value in the bend is about twice as high as the flume averaged value $\langle\langle\tau_b\rangle\rangle$ that would occur in a straight flow.

Fig. 9 shows the patterns of the normalized cross-stream circulation $(v_n^*, v_z)/U$ and downstream velocity v_s/U in the cross section of maximum cross-stream circulation at 90° and in the cross section at 180° near the exit of the bend.

Without the bubble screen, high downstream velocities (v_s) in the upper half of the water column are conveyed in the outwards direction by the cross-stream circulation cell, and lower velocities in the lower part of the water column are conveyed in the inwards direction. Averaged over the depth, outward momentum transport is dominant, resulting in an inclination of the velocity contour lines and a gradual outward shift of the core of maximum velocities. Whereas the core of maximum velocities is still at $n=-0.3$ m in the inner half of the cross section at 90°, it has reached $n=0.3$ m in the region near the outer bank in the cross section at 180°.

In the presence of the bubble screen, advective momentum transport by the curvature induced cross-stream circulation again causes the downstream velocities to increase from the inner bank in the outwards direction. At the same time, the bubble generated cross-stream circulation cell causes the downstream velocities to

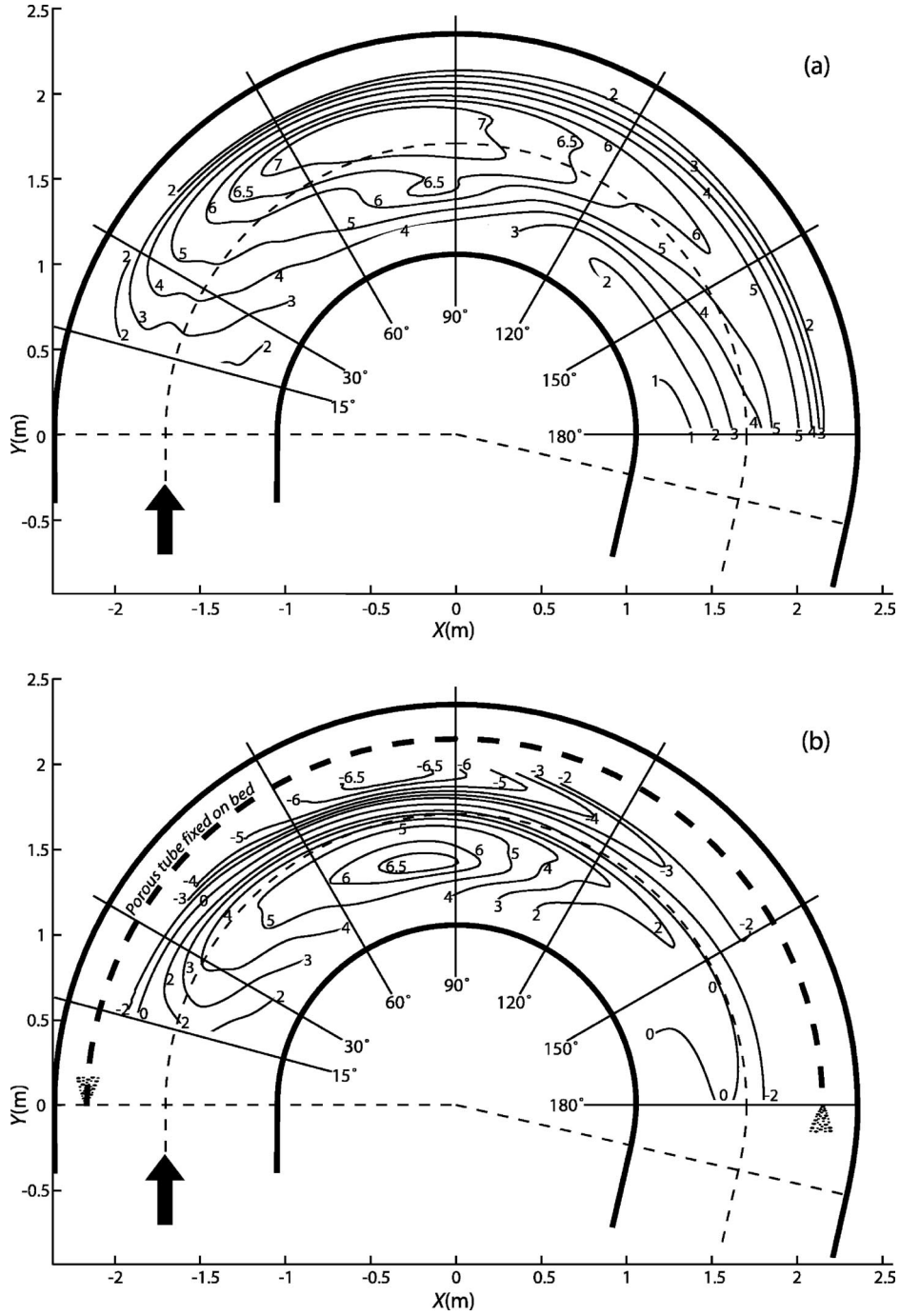

Fig. 7. Distribution of the cross-stream circulation strength, $100\langle\psi\rangle/(UH)$ in the bend: (a) reference situation without the bubble screen; (b) with the bubble screen. Bend entry/exit at the left/right. Measured cross sections at 15, 30, 60, 90, 120, 150, and 180° as indicated.

increase from the outer bank in the inwards direction in a similar way. This explains why the outward shift of the core of maximum velocities is halted at the junction of both circulation cells where the core of maximum velocities is located.

Discussion

The presented experiments demonstrate convincingly the potential of modifying the distribution of bed-shear stress and velocity by means of a bubble screen. However, some technical and economical questions need to be addressed before applying it in practice.

The following discussion will be limited to the application of bubble screens in open-channel bends.

How Would the Flow Pattern Interact with a Mobile Bed Topography?

In the reference experiment without the bubble screen, the flow has completely adapted to the imposed curvature near the bend exit, where the bed-shear stress and erosive capacity increase

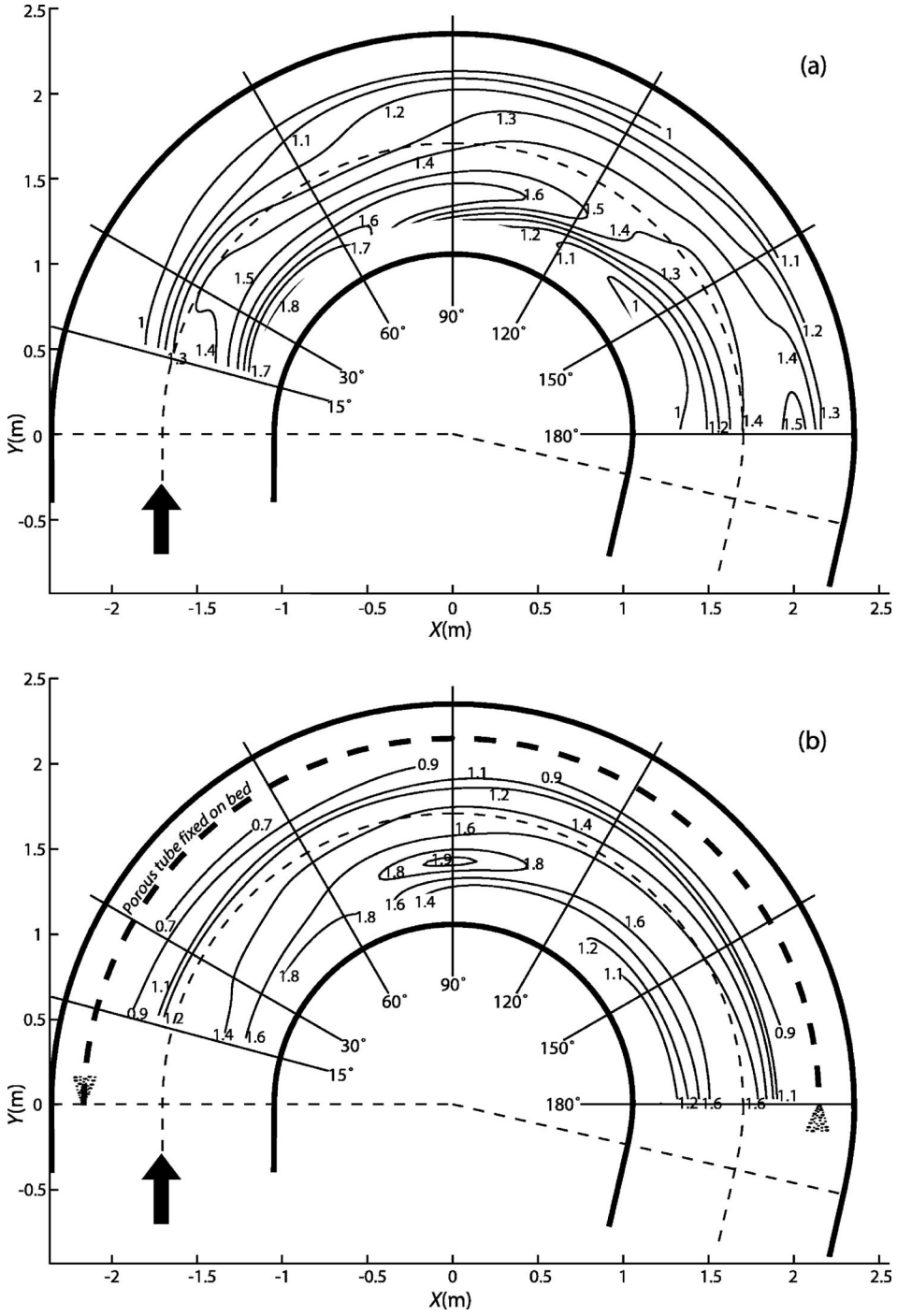

Fig. 8. Distribution of the normalized downstream bed-shear stress $\tau_{bs}/\langle\langle\tau_b\rangle\rangle$ in the bend, where $\langle\langle\tau_b\rangle\rangle$ is the flume-averaged bed-shear stress; (a) reference situation without the bubble screen; (b) with the bubble screen. Bend entry/exit at the left/right. Measured cross sections at 15, 30, 60, 90, 120, 150, and 180° as indicated.

in the outwards direction (cf. Fig. 8). They reach their maxima near the outer bank in the downflow ($v_z<0$) region, where high momentum fluid is conveyed towards the bed. If the bed were mobile, the transverse component of the bed-shear stress induced by the cross-stream circulation would transport sediments towards the inner bend. The transverse bed slope would be determined by the balance between this inward component of the bed-shear stress and the outward gravitational pull on the sediments (Odgaard 1981). The pattern of cross-stream circulation would not fundamentally change, and still consist of a curvature induced cross-stream circulation cell. Its spanwise extent and magnitude, however, would be somewhat modified over a mobile bed topography.

With the bubble screen, the bed-shear stress/erosive capacity near the bend exit is a maximum at the junction of the curvature and bubble induced cross-stream circulation cells, where the core of maximum downstream velocities (v_s) is found and where pronounced descending vertical velocities ($v_z<0$) occur. The erosive capacity decreases from this maximum value towards the bank (cf. Fig. 8). If the bed were mobile, both cross-stream circulation

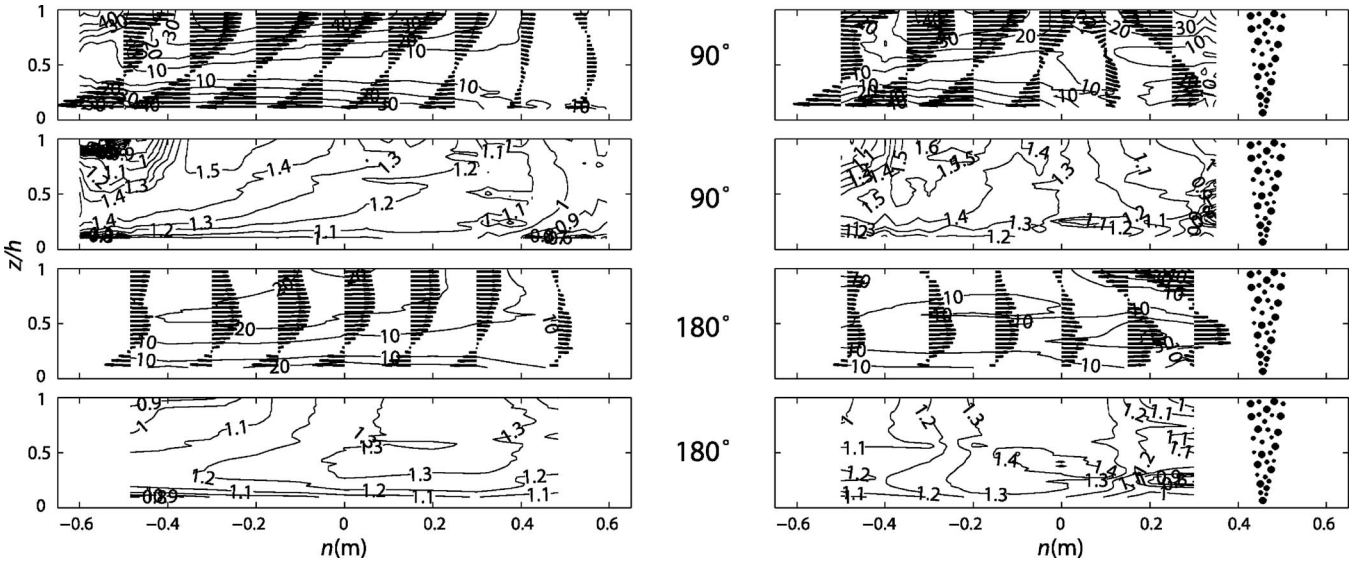

Fig. 9. Patterns of normalized cross-stream circulation $(v_n^*, v_z)/U$ (isolines show vector magnitude in [%]), and downstream velocity, v_s/U, measured in the cross sections at 90° (top) and 180° (bottom) without (left column) and with the bubble screen (right column)

cells would transport sediments towards the banks, resulting in a maximum flow depth occurring at the junction of both circulation cells.

The mobile bed topography would probably not fundamentally modify the bicellular pattern of cross-stream circulation, although the cells' spanwise extent and magnitude would probably be modified. We postulate that a favorable feedback would develop between the mobile bed and the pattern of cross-stream circulation cells, whereby the bubble induced cell widens and strengthens, and thereby weakens the curvature induced cell and pushes it in the inwards direction. The maximum flow depth, which would still occur at the separation between both cross-stream circulation cells, would hence be found further away from the outer bank, resulting in a more favorable bed topography:

- Less bend scour near the outer bank and, thus, a reduced erosive attack on that bank through toe scour.
- A more uniform depth distribution resulting in an increase of the navigable width.

Obviously, additional experiments over a mobile bed are required to confirm this postulated favorable feedback before the bubble screen technique can reliably be applied in river applications.

Contrary to other techniques used to reduce bend scour, the bubble screen technique is reversible, allowing the modification of the flow field and the bed topography in a dynamic way. The bubble screen could, for example, only be activated during discharges that are larger than the morphology building discharge, which may occur only during a restricted number of days/weeks per year. Moreover, the input of air could be favorable from an ecological point of view.

What Are the Physical Mechanisms Underlying the Bubble Generated Cross-Stream Circulation Cell? How Does the Bubble Generated Cell Depend on the Geometric Parameters, and Especially on the Water Depth H, the Curvature Ratio R/H, and the Aspect Ratio B/H?

As mentioned earlier, the strength (in terms of maximum cross-stream velocities) of the cross-stream circulation cell is mainly determined by the momentum input of the rising air bubbles. The air flux can be controlled, whereas the rising velocity of the bubbles is approximately constant at $0.24\ \mathrm{ms}^{-1}$ in the range of the applied bubble sizes (Leifer et al. 2000), independent of the flow depth and velocity. Hence, the strengths of the bubble generated cross-stream circulation cell in the laboratory experiments and in full scale rivers are probably of the same order of magnitude.

The strength of the bubble generated cell is probably only weakly influenced by the curvature ratio, as suggested by the comparison of the straight and sharply curved experiments. Its spanwise extent, however, is thought to depend on the interaction with the curvature induced cross-stream circulation cell and the mobile bed:

Table 1. Estimations of the Bubble Screen's Energy Requirements for Some Bends in the River Waal, The Netherlands

Bends in the River Waal	L [m]	R [m]	$(g/C_f)^{1/2}$ [$\mathrm{m}^{1/2}\,\mathrm{s}^{-1}$]	H [m]	B [m]	U [ms^{-1}]	UH/R [ms^{-1}]	E [Eq. (10)] [kWh/yr]
Hulhuizen	4,850	1,120	40	11.25	240	1.5	0.015	362,929
Erlecom	3,400	1,120	40	11.25	240	1.5	0.015	254,424
Nijmegen	3,500	700	40	11.25	240	1.5	0.024	134,096
St. Andries	2,600	1,370	40	10.75	240	1.5	0.012	27,670

- The strength of the curvature induced cross-stream circulation cell is in a first approximation controlled by the parameter UH/R (Rozovskii 1957; Engelund 1974; de Vriend 1977; Blanckaert and de Vriend 2003). The value of $UH/R=0.04$ ms^{-1} in the experiments is only slightly larger than in most full scale rivers. The values in the Waal near St-Andries and in the bends upstream of Nijmegen (Fig. 11) during a flood, for example, are about $UH/R=0.012$ to 0.024 ms^{-1} (cf. Table 1).
- In the section above, it was postulated that a favorable feedback with the mobile bed would enlarge the bubble induced cross-stream circulation cell.

The preliminary experiments were carried out in a rather narrow flume with a fixed bed and an aspect ratio of $B/H=8.3$. Although narrow channels occur in urbanized areas, most natural rivers of interest have a mobile bed and are shallow with an aspect ratio $B/H>20$. The bends on the Waal River near St-Andries and Nijmegen are characterized by a value of about $B/H=20$ during a flood (cf. Table 1). Although future research on the physical mechanisms underlying the generation of the bubble generated cross-stream circulation cell will have to elucidate the patterns of the curvature and bubble induced cross-stream circulation cells as a function of the aspect ratio, we postulate that the strength and spanwise extent of the bubble induced cross-stream circulation cell will hardly vary with the aspect ratio.

The above discussion on the influence of a mobile bed R/H, B/H implies that the spanwise extent of the bubble induced cross-stream circulation cell in full scale rivers with mobile beds would probably be larger than three (curved flow experiments) to four (straight flow experiments) times the water depth.

Let us assume as an approximation that the navigable width is reduced to the outer half of the cross section in open-channel bends without bubble screens, and enlarged by about $4H$ in the presence of a bubble screen. For the geometry of the River Waal during a flood (cf. Table 1), this would imply an increase of the navigable width from about 120 m to about 160 m, i.e., a significant increase of about 30%.

Is It Economically Feasible to Modify the Flow Field by Means of a Bubble Screen?

Without a bubble screen, the deformation of the bed topography is largely due to the transverse component of the bed-shear stress τ_{bn}, induced by the cross-stream circulation. Since the idea underlying the bubble screen is to counteract the deformation of the bed topography due to the cross-stream circulation, the energy requirement estimation will be based on the power of τ_{bn}, which can be approximated per unit of bed surface as

$$\frac{P}{S}=\tau_{bn}u_{bn}\left[\frac{\text{Nm/s}}{\text{m}^2}\right] \tag{4}$$

u_{bn}=transverse near bed velocity. The total power of the transverse bed-shear stress in the bend is thus

$$P=\int_{\text{bend entry}}^{\text{bend exit}}\int_{n=-B/2}^{n=B/2}\tau_{bn}u_{bn}dnds\left[\frac{\text{Nm}}{\text{s}}\right] \tag{5}$$

τ_{bn} and u_{bn} will be approximated by their maximum values in the bend, hence

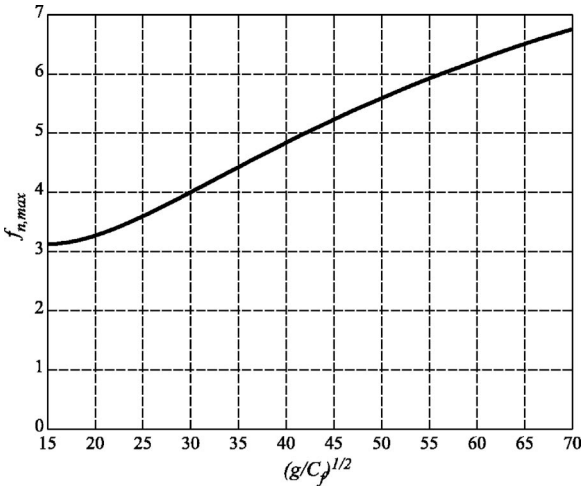

Fig. 10. Solution for $f_{n,\max}$ as a function of the Chézy friction factor $(g/C_f)^{1/2}$ according to the model of de Vriend (1977)

$$P<\tau_{bn}v^*_{n,\max}BL\left[\frac{\text{Nm}}{\text{s}}\right] \tag{6}$$

where L=bend length. The maximum value of the transverse component of the bed-shear stress can be estimated as

$$\tau_{bn,\max}=\alpha_\tau\frac{H}{R}\tau_{bs}=\alpha_\tau\frac{H}{R}\rho C_fU^2\left[\frac{\text{N}}{\text{m}^2}\right] \tag{7}$$

The coefficient α_τ is of the order of 10 (Blanckaert and de Vriend 2003). The maximum value of transverse near bed velocity will be normalized by means of a vertical form function of the transverse velocities

$$v^*_{n,\max}=UH/Rf_{n,\max} \tag{8}$$

Numerous analytical models have been proposed that yield f_n as a unique function of the channel roughness (Rozovskii 1957; Engelund 1974; de Vriend 1977). Fig. 10 gives the solution for $f_{n,\max}$ as a function of the Chézy friction coefficient C_f according to de Vriend (1977).

Hence, the total power required in the bend can be expressed as

$$P\left[\frac{\text{Nm}}{\text{s}}\right]<\alpha_\tau\rho C_f\left(\frac{H}{R}\right)^2U^3BLf_{n,\max}(C_f) \tag{9}$$

If the bubble generation is activated during d days per year, the total energy consumption per year is approximated as

$$E[\text{Nm/year}]<\alpha_\tau\rho C_f\left(\frac{H_{\max}}{R}\right)^2U^3_{\max}BLf_{n,\max}(C_f)(3{,}600\times 24)d$$

or

$$E[\text{kWh/year}]<\frac{2.8}{10^7}\alpha_\tau\rho C_f\left(\frac{H_{\max}}{R}\right)^2\times U^3_{\max}BLf_{n,\max}(C_f)(3{,}600\times 24)d \tag{10}$$

$U_{\max}$ and $H_{\max}$ are the maximum velocity and flow depth, respectively, during the time of operation. Table 1 summarizes the estimations of the energy requirements according to Eq. (10) for the bends on the River Waal in The Netherlands shown in Fig. 11, assuming 100 days of bubble generation per year.

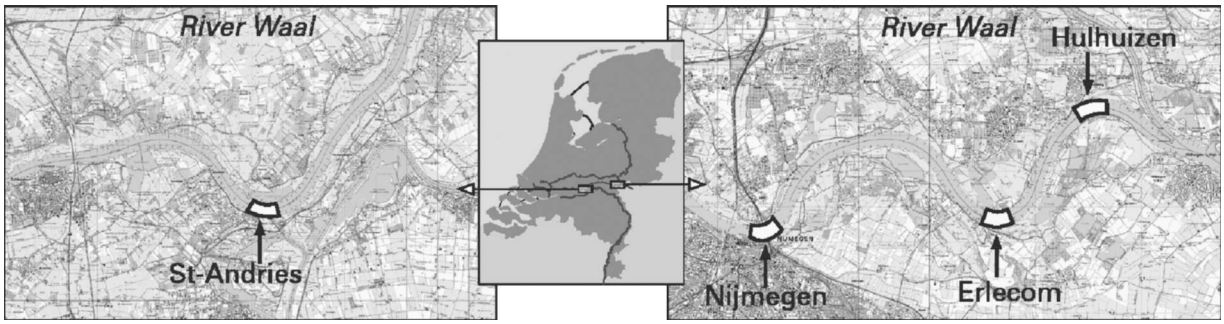

Fig. 11. Bends on the River Waal, The Netherlands, where the pronounced topography limits the navigable width (flow is from right to left)

Assuming an average price of €0.06 for 1 Kwh (on the business market), this estimation leads to relatively low operational costs. Even when taking into account energy losses (friction, pump efficiency, etc.) and building and maintenance costs, the bubble screen technique will turn out to be more economical than the present-day maintenance by means of dredging.

Conclusions

Preliminary experiments convincingly show that a bubble screen can generate cross-stream circulation in straight and curved flows, which redistributes the velocities and the bed-shear stress and thus would modify the bed topography.

In the straight flow in the laboratory, the bubble screen generates a well-defined cross-stream circulation cell that covers a spanwise extent of about four times the water depth and has maximum near-surface transverse velocities away from the bubble screen of about -0.2 ms^{-1} and maximum near-bed velocities toward it of about 0.1 ms^{-1}. These are of similar order of magnitude to typical curvature induced cross-stream circulation velocities in natural open-channel bends.

In the open-channel bend in the laboratory, the bubble generated cross-stream circulation cell is only slightly weaker in strength, but narrower with a spanwise extent of about three times the flow depth. It coexists with the counter rotating curvature induced cross-stream circulation cell, which is shifted in the inwards direction, but is hardly reduced in strength. The core of maximum downstream velocities is shifted from near the outer bank in the inwards direction to the junction of both circulation cells. Over a mobile bed, this may result in a more uniform depth distribution with a maximum depth at the junction of both circulation cells.

The bubble screen technique seems to be economically feasible in real river situations. Moreover, it has the advantage of being reversible, adjustable, and ecologically favorable. Before applying it, however, some further technical questions identified in the "Discussion" need to be resolved. Particularly, the interaction between the bubble induced flow patterns and a mobile bed, and the flow characteristics in the region between the bubble screen and the bank need to be clarified.

In addition to demonstrating the potential of the bubble screen technique, this paper provides detailed data on the 3D flow field in open-channel bends, which can be useful for validation of numerical models.

Acknowledgments

Professors Uijttewaal, Booij, and Gaskin are acknowledged for their constructive comments and suggestions.

Notation

The following symbols are used in this paper:

ADVP = acoustic Doppler velocity profiler;
B = flume width [m];
b = width of wall footing [m];
C_f = dimensionless Chézy friction coefficient;
d = mean grain size diameter [m]/days of operation per year of the bubble screen;
E = energy consumption of the bubble screen [Nm year^{-1}] or [kWh year^{-1}];
f_n = form function of the profile of the transverse velocity component;
Fr = Froude number, $\mathrm{Fr}=U/(gH)^{1/2}$ [-];
H = flume-averaged flow depth [m];
L = length of the bubble screen [m];
n = transverse reference coordinate [m]; 0 at the centerline, positive in outward direction;
P = power of the bubble screen [Nm s^{-1}];
Q = water discharge [m^3 s^{-1}];
R = centerline radius of curvature [m];
Re = Reynolds number, $\mathrm{Re}=UH/\nu$ [-];
s = downstream reference coordinate [m], positive in downstream direction;
$U=Q/(BH)$ = flume-averaged velocity [ms^{-1}];
$U_i(i=s,n,z)$ = depth-averaged velocity in i direction [ms^{-1}];
$v_i(i=s,n,z)$ = velocity in i direction [ms^{-1}];
$v_i^*(i=s,n)$ = deviation from the depth-averaged velocity component in i direction [ms^{-1}];
z = vertical reference coordinate [m], positive in upward direction;
α_τ = coefficient appearing in Eq. (7);
θ = cross section angle [deg];
ν = kinematic viscosity [m^2 s^{-1}];
ρ = density of fluid [kg m^{-3}];
τ_b = bed-shear stress;
ψ = pseudostreamfunction defined according to Eq. (3);
$\langle\ \rangle$ = depth-averaged value; and
$\langle\langle\ \rangle\rangle$ = flume-averaged value.

Subscripts

s,n,z = value in s,n,z directions;
b = value at the bed level; and
max = maximum value occurring.

References

Batchelor, G. K. (1967). *An introduction to fluid dynamics*, Cambridge Univ. Press, Cambridge, U.K.

Blanckaert, K. (2002). "Flow and turbulence in sharp open-channel bends." Ph.D. thesis No. 2545, Ecole Polytechnique Fédérale Lausanne, Switzerland, ⟨ftp://lrhmac15.epfl.ch/Pub/Thesis/Blanckaert/PhD⟩.

Blanckaert, K., and de Vriend, H. J. (2003). "Nonlinear modeling of mean flow redistribution in curved open channels." *Water Resour. Res.*, 39(12), 1375–1388.

Blanckaert, K., and de Vriend, H. J. (2004). "Secondary flow in sharp open-channel bends." *J. Fluid Mech.*, 498, 353–380.

Blanckaert, K., and Graf, W. H. (2001). "Experiments on flow in an open-channel bend. Mean flow and turbulence." *J. Hydraul. Eng.*, 127(10), 835–847.

Blanckaert, K., and Graf, W. H. (2004). "Momentum transport in sharp open-channel bends." *J. Hydraul. Eng.*, 130(3), 186–198.

Blanckaert, K., and Lemmin, U. (2006). "Means of noise reduction in acoustic turbulence measurements." *J. Hydraul. Res.*, 44(1), 3–17.

Bradshaw, P. (1987). "Turbulent secondary flows." *Annu. Rev. Fluid Mech.*, 19, 53–74.

Chow, V. T. (1959). *Open-channel hydraulics*, McGraw-Hill, New York.

Colombini, M. (1993). "Turbulence-driven secondary flows and formation of sand ridges." *J. Fluid Mech.*, 254, 701–719.

de Vriend, H. J. (1977). "A mathematical model of steady flow in curved shallow channels." *J. Hydraul. Res.*, 15(1), 37–54.

de Vriend, H. J. (1981). "Velocity redistribution in curved rectangular channels." *J. Fluid Mech.*, 107, 423–439.

Engelund, F. (1974). "Flow and bed topography in channel bends." *J. Hydr. Div.*, 100(HY11), 1631–1648.

Fargue, L. (1868). "Etude sur la corrélation entre la configuration du lit et la profondeur d'eau dans les rivières à fond mobile." *Annales des Ponts et Chaussées*.

Hersberger, D. (2002). "Wall roughness effects on flow and scouring in curved channels with gravel bed." Ph.D. thesis No. 2632, Ecole Polytechnique Fédérale Lausanne, Switzerland.

Hurther, D., and Lemmin, U. (1998). "A constant beamwidth transducer for three-dimensional Doppler profile measurements in open channel flow." *Meas. Sci. Technol.*, 9(10), 1706–1714.

Ikeda, S., and Nishimura, T. (1985). "Bed topography in bends of sand-slit rivers." *J. Hydraul. Eng.*, 111(11), 1397–1411.

Jaeggi, M. N. R. (1984). "Formation and effects of alternate bars." *J. Hydraul. Eng.*, 110(2), 142–156.

Kikkawa, H., Ikeda, S., and Kitagawa, A. (1976). "Flow and bed topography in curved open channels." *J. Hydr. Div.*, 102(HY9), 1327–1342.

Knaapen, M. A. F., Hulscher, S. J. M. H., de Vriend, H. J., and van Harten, A. (2001). "Height and wavelength of alternate bars in rivers: Modeling vs. laboratory experiments." *J. Hydraul. Res.*, 39(2), 147–153.

Leifer, I., Patro, R. K., and Bowyer, P. (2000). "A study on the temperature variation of rise velocity for large clean bubbles." *J. Atmos. Ocean. Technol.*, 17(10), 1392–1402.

Lemmin, U., and Rolland, T. (1997). "Acoustic velocity profiler for laboratory and field studies." *J. Hydraul. Eng.*, 123(12), 1089–1098.

Nezu, I., and Nakagawa, H. (1984). "Cellular secondary currents in straight conduit." *J. Hydraul. Eng.*, 110(2), 173–193.

Nezu, I., and Nakagawa, H. (1993). *Turbulence in open-channel flows*, IAHR Monograph, Balkema, Rotterdam, The Netherlands.

Odgaard, A. J. (1981). "Transverse bed slope in alluvial channel bends." *J. Hydr. Div.*, 107(HY12), 1677–1693.

Odgaard, A. J. (1984). "Flow and bed topography in alluvial channel bend." *J. Hydraul. Eng.*, 110(4), 521–536.

Odgaard, A. J., and Spoljaric, A. (1986). "Sediment control by submerged vanes." *J. Hydraul. Eng.*, 112(12), 1164–1181.

Odgaard, A. J., and Wang, Y. (1991). "Sediment management with submerged vanes. I: Theory." *J. Hydraul. Eng.*, 117(3), 267–283.

Roca, M., Martin-Vide, J. P., and Blanckaert, K. (2006). "Reduction of bend scour by an outer bank footing. Footing design and bed topography." *J. Hydraul. Eng.*, 133(2), 139–147.

Rozovskii, I. L. (1957). "Flow of water in bends of open channels." *Ac. Sc. Ukr. SSR, Isr. Progr. Sc. Transl.*, Jerusalem, Israel.

Schielen, R., Doelman, A., and Deswart, H. E. (1993). "On the nonlinear dynamics of free bars in straight channels." *J. Fluid Mech.*, 252, 325–356.

Sloff, C. J., Mosselman, E., and Sieben, J. (2006). "Effective use of nonerodible layers for improving navigability." *Proc., River Flow 2006*, R. M. L. Ferreira, E. C. T. L. Alves, J. G. A. B. Leal, and A. H. Cardoso, eds., Taylor and Francis Group, London, Vol. II, 1211–1220.

Struiksma, N. (1985). "Prediction of 2-D bed topography in rivers." *J. Hydraul. Eng.*, 111(8), 1169–1182.

Thomson, W. (1876). "On the origin of windings of rivers in alluvial plains, with remarks on the flow of water round bends in pipes." *Proc. R. Soc. London*, 25, 5–8.

Whiting, P. J., and Dietrich, W. E. (1993). "Experimental studies of bed topography and flow patterns in large-amplitude meanders. I: Observations." *Water Resour. Res.*, 29(11), 3605–3614.